
FrameVGGT: Frame Evidence Rolling Memory for streaming VGGT

Zhisong Xu

Institute of Industrial Science
The University of Tokyo
Tokyo, Japan

zhisongxu@cvl.iis.u-tokyo.ac.jp

Takeshi Oishi

Institute of Industrial Science
The University of Tokyo
Tokyo, Japan

oishi@cvl.iis.u-tokyo.ac.jp

Abstract

Streaming Visual Geometry Transformers such as StreamVGGT enable strong online 3D perception but suffer from unbounded KV-cache growth, which limits deployment over long streams. We revisit bounded-memory streaming from the perspective of geometric support. In geometry-driven reasoning, memory quality depends not only on how many tokens are retained, but also on whether the retained memory still preserves sufficiently coherent local support. This suggests that token-level retention may become less suitable under fixed budgets, as it can thin the evidence available within each contributing frame and make subsequent fusion more sensitive to weakly aligned history. Motivated by this observation, we propose FrameVGGT, a frame-driven rolling explicit-memory framework that treats each frame’s incremental KV contribution as a coherent evidence block. FrameVGGT summarizes each block into a compact prototype and maintains a fixed-capacity mid-term bank of complementary frame blocks under strict budgets, with an optional lightweight anchor tier for rare prolonged degradation. Across long-sequence 3D reconstruction, video depth estimation, and camera pose benchmarks, FrameVGGT achieves favorable accuracy–memory trade-offs under bounded memory, while maintaining more stable geometry over long streams.

1 Introduction

Dense 3D reconstruction from images is a core capability for augmented reality, robotics, and embodied AI [1, 2, 3, 4, 5]. Classical SfM/MVS pipelines achieve high fidelity through explicit geometric optimization [6, 7, 8], but are typically multi-stage and computationally expensive. Recent geometric foundation models have shifted this paradigm toward feed-forward inference: **DUS_t3R** [9] predicts dense correspondences and geometry directly, **MASt_{3R}** [10] improves multi-view consistency and scalability, and **VGGT** [11] unifies cross-view interaction with Transformers to jointly predict cameras, depth/points, and tracking under a fixed-size multi-view input.

Extending such models to *online* long-horizon streams, however, exposes a fundamental tension. Stable geometric reasoning benefits from historical evidence, yet caching all past context causes memory and latency to grow with sequence length. Existing streaming designs typically make one of two compromises. *Implicit state compression* (e.g., CUT3R, TTT3R) [12, 13] bounds resource usage by folding history into a latent state, but the compression bottleneck can weaken long-range constraints and induce drift. *Explicit history accumulation* (e.g., StreamVGGT) [14] preserves richer temporal support by caching past KV states, but its footprint grows unbounded over long streams.

To reconcile explicit memory with bounded resources, **InfiniteVGGT** [15] introduces rolling cache control via token retention based on attention-independent proxies such as key-space diversity,

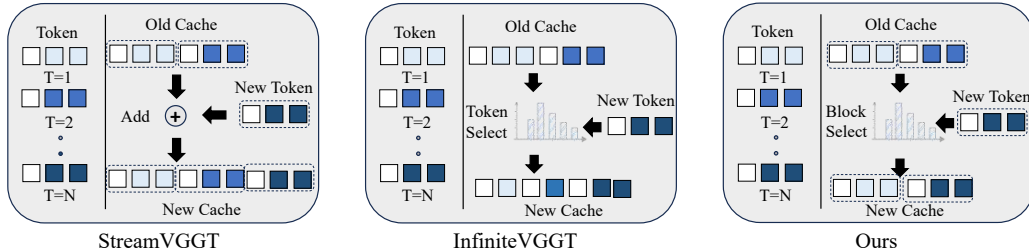


Figure 1: Memory organization strategies for streaming VGGT under a fixed budget. StreamVGGT keeps the full cache, InfiniteVGGT applies token-level bounded retention, and FrameVGGT applies support-aligned frame/block-level bounded retention.

avoiding attention-matrix materialization while remaining compatible with efficient kernels. Despite its efficiency, *token-level* retention can become poorly matched to long-horizon geometric streaming under bounded memory. The issue is not merely how many memory entries are kept, but whether bounded memory still preserves the *coherent support* needed for geometric estimation. In geometry-driven prediction, depth and pose depend less on isolated salient tokens than on locally compatible multi-view evidence. Under a fixed budget, token-level pruning can progressively thin within-frame support and fragment evidence across space and time as the stream grows. As a result, downstream retrieval and fusion operate on thinner and less mutually consistent support, increasing sensitivity to mismatch, noise, and incidental saliency. The bottleneck is therefore not raw token count alone, but a *granularity mismatch*: token-level compression acts on units finer than the support units required for stable geometric estimation, as illustrated in Fig. 1.

Motivated by this observation, we propose **FrameVGGT**, a **support-aligned rolling explicit-memory** framework for robust online 3D geometry. Instead of treating the Transformer KV cache as a shared pool of independent tokens, FrameVGGT groups each frame’s incremental cache contribution into a coherent evidence block and maintains a fixed-capacity mid-term bank of complementary frame blocks under a strict budget. The central idea is to align the *retention unit* of bounded memory with the *support unit* of geometric estimation, thereby preserving more coherent within-frame evidence and more complementary cross-view support over long horizons for depth, pose, and reconstruction. Importantly, this is not image-level keyframe selection; rather, it is a reorganization of the *internal Transformer KV cache* into support-aligned evidence units for bounded streaming inference.

For additional robustness, we further include a lightweight **global anchor tier** that retains a small number of sparse, persistent reference frames. Whereas the mid-term bank serves as the primary bounded support mechanism over recent-to-mid horizons, anchors provide occasional long-range references during challenging intervals such as rapid rotation, weak parallax, or severe occlusion. Because the anchor tier occupies only a small fraction of the total memory budget, it improves robustness in difficult cases with little additional overhead.

Contributions. We make three contributions:

- (1) **A support-aligned bounded explicit-memory formulation for long-horizon geometry.** We identify *retention granularity* as an important design axis in bounded streaming geometry, and introduce a rolling explicit-memory formulation that aligns the retention unit with the support unit of geometric estimation, improving long-horizon depth, pose, and reconstruction under the same memory budget.
- (2) **A proxy-based analysis of granularity mismatch in geometric streaming.** We provide an analytical perspective on how token-level compression can become poorly matched to bounded long-horizon geometry, characterizing three coupled failure modes: support thinning, spatio-temporal decoupling, and fusion brittleness under weak redundancy.
- (3) **A multi-timescale memory design with lightweight global anchoring.** We show that augmenting bounded mid-term support with a small set of sparse, persistent reference frames provides a simple robustness extension for challenging intervals, improving stability with little additional memory overhead.

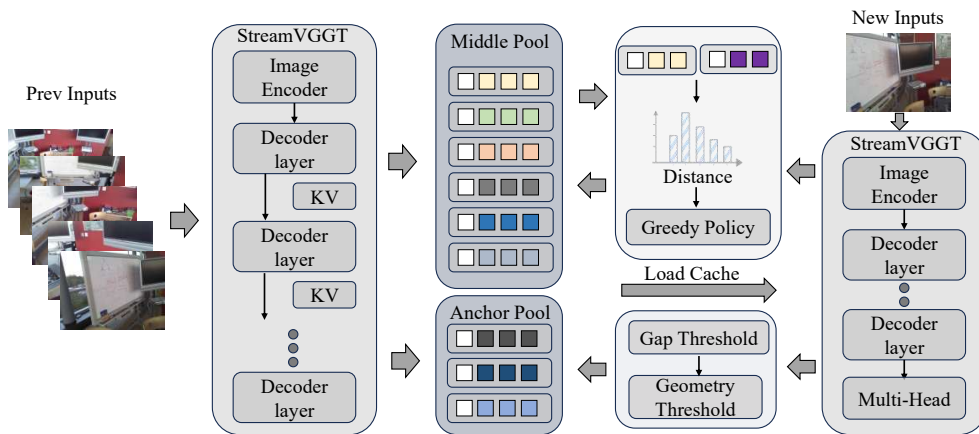


Figure 2: Pipeline of FrameVGGT. Previous inputs are encoded to form per-layer KV blocks, which are managed by a middle-term pool using a distance-based greedy selection policy, and an optional anchor pool gated by gap and geometry thresholds. The selected cache is loaded to condition new inputs for streaming inference.

2 Related Work

2.1 Geometry-based Reconstruction

Classical 3D reconstruction relies on explicit geometric optimization. Offline pipelines such as SfM and MVS jointly estimate camera poses and scene structure over all views [16, 17, 18, 19], but require full-scene access and expensive global optimization. Online systems such as SLAM update motion and maps incrementally [20, 21], yet typically focus on sparse or semi-dense representations, making dense long-horizon reconstruction under strict budgets challenging.

2.2 Learning-based Reconstruction with Fixed-size Inputs

Recent learning-based methods infer geometry in a feed-forward manner from images and jointly predict cameras, depth, and correspondences across multiple views. However, these models are designed for fixed-size inputs, with memory and compute growing rapidly with the number of views. Several extensions improve scalability through sub-map decomposition [22], anchor-based representations [23], or token-level acceleration, but remain largely batch-oriented.

2.3 Learning-based Reconstruction under Streaming Constraints

Streaming methods process frames online while maintaining history. *Explicit-memory* approaches cache features, tokens, or states for reuse [24, 25, 26], but naive accumulation leads to growing memory and latency. *Implicit-state* approaches compress history into bounded latent states, often weakening long-range constraints and causing drift. Windowed methods restrict computation to local temporal neighborhoods [27], stabilizing runtime but limiting long-horizon consistency.

Most prior work focuses on how much history to keep or how to bound computation. By contrast, we focus on how bounded memory is organized inside geometry transformers such as VGGT. In particular, token-level retention can be mismatched to geometry-driven reasoning, where stable inference depends on coherent support from mutually compatible observations rather than isolated retained tokens.

3 Method

3.1 Problem Formulation: Streaming Geometry with a Bounded KV Cache

We consider online geometric inference over an unbounded observation stream $\mathcal{I} = \{I_t\}_{t \geq 1}$, where the model predicts geometric outputs y_t sequentially. Its only persistent state is the layer-wise Transformer key-value (KV) cache. For each layer l , the cache at time t is

$$C_t^{(l)} = (K_t^{(l)}, V_t^{(l)}), \quad K_t^{(l)}, V_t^{(l)} \in \mathbb{R}^{B \times H \times T_t^{(l)} \times D}, \quad (1)$$

where $T_t^{(l)}$ is the number of cached tokens. As new entries $\Delta C_t^{(l)}$ are appended over time,

$$C_t^{(l)} = C_{t-1}^{(l)} \oplus \Delta C_t^{(l)}, \quad (2)$$

the cache grows monotonically with sequence length. Without compression, this leads to unbounded memory and increasing inference cost, which is incompatible with long-horizon streaming.

We therefore study bounded streaming inference, where a compressed rolling cache

$$\hat{C}_t = \{\hat{C}_t^{(l)}\}_l \quad (3)$$

is maintained under strict per-layer budgets

$$\|\hat{C}_t^{(l)}\|_0 \leq B^{(l)}, \quad \forall t, \quad (4)$$

where $B^{(l)}$ is the maximum cache capacity of layer l . This yields a constrained online memory-selection problem: only a bounded subset of past evidence can remain available to support future inference.

Crucially, bounded streaming memory is governed not only by how much context is retained, but also by the *granularity* of retention under a fixed budget. Even with the same nominal memory footprint, different retention units can produce markedly different support structures in the retained cache. This distinction is especially important for geometry, where depth, pose, and reprojection consistency depend less on isolated salient tokens than on groups of mutually compatible observations. Such support relies on sufficient redundancy, spatial extent, and cross-view overlap to stabilize local estimation. This motivates a support-centric view of bounded memory: the value of retained context lies not in token count alone, but in whether the retained cache continues to preserve coherent geometric support.

3.2 Principle: Preserve Support-Unit Integrity, Not Token Count Alone

We therefore view bounded streaming geometry as a constrained *support-preservation* problem rather than a token-retention problem. The core trade-off is not merely between memory and accuracy, but between compression and *support-unit integrity*. An effective retention policy should preserve coherent support units—groups of observations that jointly provide sufficient parallax, correspondence, and spatial diversity to constrain local geometry—rather than maximize global token coverage in an unstructured sense.

This perspective reveals a structural weakness of token-level pruning. Under a fixed budget, fine-grained retention can spread memory across an increasingly long temporal horizon while leaving only a thin subset of evidence within each contributing frame. As a result, the nominal token budget may remain fixed even as the retained support in local temporal neighborhoods becomes progressively weaker. For geometric estimation, this is critical: repeated observations are often not disposable redundancy, but part of the support needed for stable triangulation, pose estimation, and long-range correction. Once the retained evidence becomes too sparse, too clustered, or too weakly coupled, it may no longer provide a sufficiently non-degenerate basis for stable inference.

A second difficulty arises during memory fusion. When support integrity is weakened, subsequent key-query fusion depends on fewer surviving observations and becomes more sensitive to mismatch, noise, or accidental saliency. The cache may therefore remain numerically active while becoming less aligned with the support required by the current inference step. The resulting failure mode is not only one of memory scarcity, but also one of *support misalignment*: the retained memory satisfies the budget while no longer preserving the relational structure on which geometric reasoning depends.

These observations motivate a simple but task-aligned principle: the retention unit should be aligned with the natural granularity of geometric evidence. By aligning the pruning unit with the support unit used by downstream reasoning, bounded memory can better preserve within-frame compatibility, spatial coverage, and local parallax structure over long streams.

Appendix A develops this intuition through a proxy-based analysis from two complementary viewpoints. First, it shows how token-level compression can induce *support thinning* and *spatio-temporal decoupling*, weakening the multi-view constraints required for stable geometry. Second, it analyzes how weak redundancy can make downstream fusion more brittle, using a contrast statistic in key space as an empirical indicator of bias amplification under bounded memory. Together, these analyses help explain why token-level retention becomes increasingly less suitable as the stream grows, even when the cache size remains fixed.

3.3 Bounded Rolling Memory: Middle Bank with Sparse Anchors

Guided by the support-centric view above, we formulate bounded memory as a *retention-granularity* problem. Rather than selecting isolated tokens from a mixed cache, we retain each frame’s incremental KV contribution as a coherent evidence block. Memory is organized into a **middle bank** for primary bounded reasoning and a sparse **anchor tier** for occasional long-range references in difficult cases. As shown in Fig. 2, previous inputs are converted into per-layer KV blocks and managed at the block level, aligning internal cache organization with the support units used by downstream geometric reasoning.

Middle bank. Our central design choice is to make the frame-wise KV block, rather than an individual token, the atomic unit of retention. For each time step t and layer l , let $B_t^{(l)}$ denote the newly appended cache block produced by frame t , with keys $\{K_{t,h,\tau}^{(l)}\}_{h=1,\tau \in T_t}^H$, where T_t indexes the tokens introduced at time t . To compare frame blocks efficiently without materializing attention matrices, we summarize each block by a lightweight key-space prototype

$$v_t^{(l)} = \frac{1}{H |T_t|} \sum_{h=1}^H \sum_{\tau \in T_t} K_{t,h,\tau}^{(l)}. \quad (5)$$

After ℓ_2 normalization, $\bar{v}_t^{(l)} = v_t^{(l)} / \|v_t^{(l)}\|_2$, we define inter-block distance by cosine dissimilarity

$$d(B_i^{(l)}, B_j^{(l)}) = 1 - \langle \bar{v}_i^{(l)}, \bar{v}_j^{(l)} \rangle. \quad (6)$$

When the middle bank exceeds its capacity B_M , we retain a representative subset by approximately solving the metric k -center objective

$$\min_{S \subseteq M_t, |S| \leq B_M} \max_{B \in M_t} \min_{B' \in S} d(B, B'), \quad (7)$$

where M_t is the current candidate pool of frame blocks. This favors complementary frame blocks over near-duplicate observations, which frequently arise under slow motion or limited viewpoint change.

In practice, we use an incremental greedy farthest-first update initialized from the most recent block to preserve immediate relevance. For each candidate block $B \in M_t$, we maintain the running coverage score

$$m(B) = \min_{B' \in S} d(B, B'), \quad (8)$$

which measures how far B remains from the currently selected subset S . Initialization sets S to contain the most recent block. Each subsequent step adds the block with the largest current $m(B)$, after which the score is updated by

$$m(B) \leftarrow \min(m(B), d(B, B_{\text{new}})), \quad \forall B \in M_t. \quad (9)$$

This yields a simple online rule for maintaining a complementary set of frame blocks under the bounded middle-bank budget.

Conceptually, our method does not perform classical keyframe selection over images or poses; rather, it reorganizes the retention unit of bounded Transformer memory itself. By operating directly on frame-wise KV blocks, it preserves support structure inside the model’s internal cache rather than only at the input or trajectory level. Selection is performed independently for each layer, allowing different layers to maintain memory structures appropriate to their own representation scale.

Anchor tier. In addition to the middle bank, we maintain a sparse **anchor tier** operating at a much longer temporal timescale. Whereas the middle bank provides the primary bounded support for ongoing inference, anchors preserve a small number of persistent references that may remain useful when local rolling memory becomes unreliable, e.g., under blur, occlusion, weak parallax, or rotation-dominant motion.

Anchors are promoted only when a minimum elapsed gap is satisfied,

$$\Delta_t = t - t_{\text{last}} \geq G,$$

which keeps them temporally sparse. Among eligible candidates, promotion is guided by two simple criteria: geometric reliability,

$$\Phi(i) = q_i \cdot s_i, \tag{10}$$

where q_i is model confidence and s_i is a sharpness score, and novelty relative to existing anchors,

$$\nu(i) = \min_{a \in A_t} (1 - \langle \bar{p}_i, \bar{p}_a \rangle), \tag{11}$$

where \bar{p}_i is the normalized pose signature of candidate i . We keep at most B_A anchors, permanently retain the first frame, and apply FIFO eviction to the remaining slots.

Overall memory organization. The resulting memory has a simple division of labor. The middle bank provides the primary bounded context for ongoing geometric reasoning by retaining complementary frame-level evidence blocks. The anchor tier adds a small number of persistent longer-range references that improve robustness in difficult segments. Together, they turn bounded streaming memory from token-level buffering into a more structured internal cache that better preserves the support needed for long-horizon geometric inference.

4 Experiments

4.1 Experimental Setup

We evaluate FrameVGGT on three complementary tasks—*online 3D reconstruction*, *video depth estimation*, and *monocular camera pose estimation*—to assess geometric accuracy, long-horizon stability, and bounded-resource efficiency. Across all experiments, we follow a strict *resource-controlled protocol*: pretrained backbone weights, frame sampling, and the inference pipeline are fixed, and we vary only the rolling-memory configuration to emulate different GPU memory budgets in a controlled and reproducible manner. This isolates the effect of memory organization itself and makes the comparison focus on retention policy rather than training or architectural changes. Unless otherwise stated, all methods operate under comparable KV-cache budgets, ensuring that performance differences primarily reflect the memory retention strategy rather than raw memory capacity.

In addition to prior streaming baselines, we also evaluate alternative policy-level memory strategies under the same backbone and total budget, including recency-biased bounded buffering and anchor-based repartitioning. These controlled comparisons help distinguish gains from simple bounded heuristics from gains due to support-aligned memory organization.

Memory-budget sweep. We parameterize rolling memory by the mid-term capacity M , defined as the maximum number of refreshable frame-evidence blocks retained in the mid-term bank. We sweep $M \in \{12, 16, 20, 24\}$ while holding all other components fixed. This evaluates how support-aligned memory scales under increasingly relaxed budgets and whether the gains saturate once additional capacity provides diminishing geometric utility.

Global-anchor diagnostic. To study whether sparse persistent references help under geometrically degraded intervals, we compare **24 mid-term + 0 anchor** against **20 mid-term + 4 anchor** under the same total memory budget. Both settings use identical backbone weights, frame sampling, and all other hyperparameters. This diagnostic isolates the role of anchors as a lightweight fallback for difficult conditions such as blur, occlusion, or weak-parallax motion.

Table 1: Reconstruction results on 7-Scenes and NRGBD. Best results are shown in bold.

Method	7-Scenes						NRGBD					
	Acc \downarrow	Acc $_{med}\downarrow$	Comp \downarrow	Comp $_{med}\downarrow$	NC \uparrow	NC $_{med}\uparrow$	Acc \downarrow	Acc $_{med}\downarrow$	Comp \downarrow	Comp $_{med}\downarrow$	NC \uparrow	NC $_{med}\uparrow$
CUT3R	0.181	0.127	0.095	0.0327	0.525	0.531	0.322	0.237	0.128	0.0334	0.553	0.566
Point3R	0.063	0.026	0.031	0.0150	0.559	0.589	0.113	0.048	0.037	0.0060	0.621	0.696
TTT3R	0.060	0.035	0.028	0.0050	0.560	0.588	0.161	0.082	0.093	0.0147	0.602	0.654
InfiniteVGGT	0.041	0.016	0.024	0.0047	0.561	0.593	0.078	0.049	0.035	0.0069	0.647	0.757
Ours(12)	0.035	0.013	0.020	0.0048	0.562	0.594	0.054	0.036	0.031	0.0068	0.656	0.764
Ours(16)	0.033	0.010	0.019	0.0044	0.564	0.597	0.053	0.035	0.030	0.0061	0.663	0.773
Ours(20)	0.027	0.008	0.018	0.0038	0.563	0.595	0.053	0.036	0.033	0.0067	0.661	0.776
Ours(24)	0.028	0.009	0.019	0.0040	0.564	0.598	0.054	0.035	0.030	0.0060	0.670	0.782

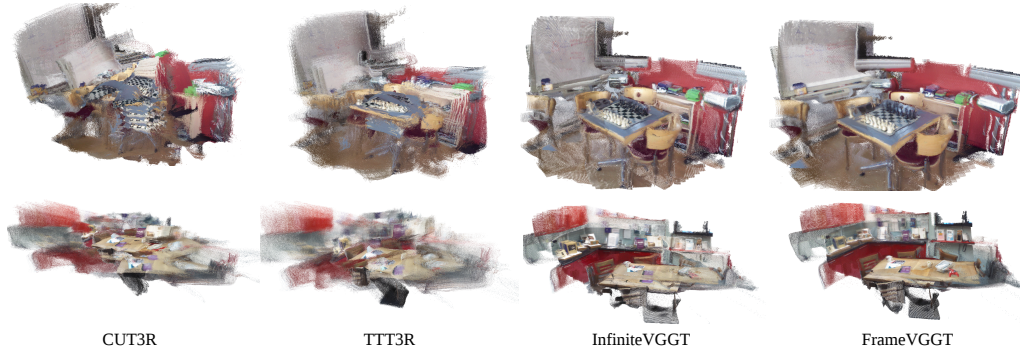


Figure 3: Reconstruction visualization comparison on the 7scenes dataset. InfiniteVGGT exhibits some floats over extended sequences, while our method maintains a more stable result.

Recency-versus-mid-term ablation. We evaluate a recency-biased memory policy by enforcing a **Recent- K** buffer that always reserves capacity for the last K frames, while assigning the remaining budget to the mid-term bank. We test $K \in \{2, 4, 6\}$ and compare these allocations against the default **mid-term-only** policy under the same total budget. This provides a controlled baseline for the common heuristic of prioritizing temporal proximity. However, as shown in our results, such recency-biased allocation consistently underperforms: reserving memory for the most recent frames over-allocates capacity to highly redundant adjacent observations and reduces the complementary mid-term support needed for stable long-horizon geometry.

Implementation details. FrameVGGT is implemented as a plug-and-play inference-time rolling-memory mechanism on top of a fixed pretrained backbone, requiring neither retraining nor fine-tuning. The reported memory corresponds to the effective KV-cache footprint during streaming inference. We report standard evaluation metrics and follow the conventional protocol of each benchmark. All experiments are conducted on a single NVIDIA RTX A6000 GPU.

4.2 3D Reconstruction

Protocol and metrics. We evaluate 3D reconstruction on 7-SCENES and NRGBD [28, 29], reporting Accuracy (Acc, \downarrow), Completeness (Comp, \downarrow), and Normal Consistency (NC, \uparrow). Following standard practice, we keep frame sampling fixed across methods and evaluate full long-horizon sequences with stride 2 (up to 1000 frames), enabling controlled comparisons with prior streaming baselines and alternative memory policies under bounded-memory inference.

Effect of mid-term capacity. Tab. 1 and Fig. 3 show that increasing the mid-term capacity M consistently improves long-horizon reconstruction under bounded resources. Compared with token-level streaming baselines, our support-aligned memory yields cleaner geometry and fewer artifacts such as floating structures or duplicated surfaces. It also achieves a better accuracy-memory trade-off: our settings with 12/16/20/24 mid-term blocks use approximately $\{1.9, 2.4, 3.0, 3.7\}$ GB of KV-cache memory, whereas InfiniteVGGT requires about 6.9 GB under comparable settings. Unless otherwise

Table 2: Performance comparison across anchor configurations. Best results are shown in bold.

Scene	Anchor=0						Anchor=4					
	Acc↓	Acc _{med} ↓	Comp↓	Comp _{med} ↓	NC↑	NC _{med} ↑	Acc↓	Acc _{med} ↓	Comp↓	Comp _{med} ↓	NC↑	NC _{med} ↑
office/seq-09	0.0429	0.0088	0.0126	0.0044	0.5627	0.6085	0.0275	0.0088	0.0119	0.0044	0.5758	0.6163
stairs/seq-01	0.1392	0.0556	0.0915	0.0077	0.5411	0.5585	0.1250	0.0521	0.0932	0.0081	0.5565	0.5726

Table 3: Reconstruction results on 7-Scenes and NRGBD. Best results are shown in bold.

Method	7-Scenes						NRGBD					
	Acc↓	Acc _{med} ↓	Comp↓	Comp _{med} ↓	NC↑	NC _{med} ↑	Acc↓	Acc _{med} ↓	Comp↓	Comp _{med} ↓	NC↑	NC _{med} ↑
Recent-0	0.033	0.010	0.019	0.0044	0.564	0.597	0.053	0.035	0.030	0.0061	0.663	0.773
Recent-2	0.037	0.013	0.020	0.0044	0.562	0.593	0.056	0.040	0.031	0.0070	0.656	0.768
Recent-4	0.053	0.017	0.024	0.0050	0.558	0.587	0.066	0.045	0.031	0.0073	0.637	0.734
Recent-6	0.069	0.025	0.027	0.0050	0.555	0.583	0.085	0.059	0.034	0.0080	0.623	0.707

noted, all methods operate under comparable KV-cache budget settings, so the comparison primarily reflects differences in memory organization rather than unequal memory allocation.

The gains from increasing M can be attributed to stronger *constraint diversity*: a larger mid-term bank retains more complementary mid-horizon evidence when recent observations alone are insufficient. The improvement gradually saturates at larger budgets, as additional blocks increasingly overlap with existing evidence and contribute diminishing returns.

Global-anchor diagnostic. Tab. 2 reports a targeted diagnostic of the global anchor tier on challenging sequences. The results suggest that anchors help not by simply retaining more old history, but by adding a sparse set of persistent references when the rolling mid-term context becomes unreliable. This is particularly useful under blur, occlusion, or weak-parallax motion, where a few stable long-range references can help maintain global consistency. By contrast, overly aggressive anchor allocation can hurt visually stable sequences, indicating that anchors are most useful as a lightweight fallback rather than a replacement for the mid-term bank. This also suggests that simply retaining more long-range history is not sufficient by itself: without selective allocation and compatibility with the actively useful mid-term context, additional old evidence can dilute bounded memory rather than improve reconstruction.

Recent vs. mid-term evidence. Tab. 3 shows that forcing a Recent- K buffer does not reliably improve reconstruction and often degrades it. Compared with our default policy and other policy-level baselines, FIFO-style recency tends to over-allocate memory to near-duplicate adjacent frames while displacing more complementary mid-term support. This reduces effective baseline diversity and weakens robustness over long horizons. More importantly, when viewed together with the anchor diagnostic, these results rule out two simple alternatives: performance is not improved by prioritizing recent history alone, nor by naively retaining more long-range history in a generic sense. Together, these results suggest that bounded streaming reconstruction depends less on raw history length or recency alone than on preserving complementary frame-level support under a fixed memory budget.

4.3 Video Depth Estimation

Protocol and metrics. We evaluate streaming video depth estimation on BONN [30] over sequences of up to 500 frames, reporting Abs Rel (\downarrow) and $\delta < 1.25$ (\uparrow) after per-sequence scale alignment. The evaluation protocol is kept fixed across memory settings for controlled comparison. Compared with reconstruction and pose, prolonged severe degradation is less common on this benchmark, so the anchor tier mainly acts as a safety margin and empirically behaves similarly to the mid-term-only setting on most sequences.

Effect of mid-term capacity. Tab. 4 shows that our frame-level rolling memory maintains strong depth accuracy under bounded budgets. Increasing the mid-term capacity M yields modest but consistent improvements in Abs Rel, while $\delta < 1.25$ remains uniformly high across settings. This suggests that additional mid-term context provides complementary geometric support when recent observations alone are insufficient, but that the benefit naturally saturates once the current frame

Table 4: Video depth estimation results on Bonn. Best results are shown in bold.

Method	Abs Rel \downarrow	$\delta < 1.25 \uparrow$
CUT3R	0.0831	0.9402
Point3R	0.0809	0.9513
TTT3R	0.0752	0.9587
InfiniteVGGT	0.0560	0.9802
Ours (12)	0.0526	0.9793
Ours (16)	0.0525	0.9801
Ours (20)	0.0514	0.9799
Ours (24)	0.0512	0.9799

Table 5: Recent ablation on Bonn under a fixed total budget ($M_{\text{total}}=16$). Recent-0 corresponds to Ours ($M=16$). Best results are shown in bold.

Sliding Window	Abs Rel \downarrow	$\delta < 1.25 \uparrow$
Recent-0	0.0525	0.9801
Recent-2	0.0535	0.9794
Recent-4	0.0562	0.9788
Recent-6	0.0589	0.97804

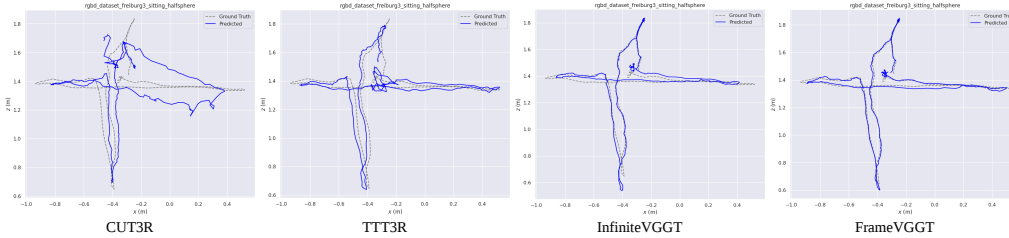


Figure 4: Pose visualization comparison on the TUM dataset. InfiniteVGGT exhibits noticeable long-horizon drift over extended sequences, while our method maintains a more stable trajectory estimation.

already has adequate local support. Overall, the results indicate that support-aligned memory is sufficient to preserve reliable depth cues over long horizons without requiring unbounded cache growth.

Recent vs. mid-term evidence. Consistent with reconstruction, enforcing a Recent- K buffer does not improve depth accuracy and instead gradually degrades performance as K increases (Tab. 5). Adjacent frames often contribute highly overlapping constraints, so a larger recent buffer over-allocates memory to near-duplicate evidence while reducing capacity for more complementary mid-term support. This lowers the diversity of usable constraints and weakens recovery from locally ambiguous observations. The same trend across reconstruction and depth further supports our central claim: effective streaming memory should preserve complementary support structure rather than prioritize recency alone.

4.4 Camera Pose Estimation

Protocol and metrics. We evaluate streaming camera pose estimation on TUM-DYNAMICS [31] using sequences of up to 300 frames. We report ATE, RPE_{trans} , and RPE_{rot} (all \downarrow) after Sim(3) Umeyama alignment, used only for global similarity normalization without any refinement. As in depth estimation, the anchor tier mainly acts as a hard-case safety margin and does not provide systematic gains on this dataset.

Effect of mid-term capacity. Tab. 6 and Fig. 4 show that pose estimation is more sensitive to tight memory budgets than depth, since insufficient mid-horizon support is directly accumulated into long-horizon trajectory drift. Compared with token-level streaming baselines, our frame-level rolling memory preserves more complementary support, leading to lower ATE and RPE over extended sequences.

Increasing the mid-term capacity M consistently improves pose accuracy, with most gains achieved at moderate budgets and diminishing returns thereafter. This suggests that additional mid-term memory mainly helps by retaining complementary viewpoints and baselines beyond the immediate neighborhood of the current frame. Once the dominant support gaps are covered, further retained blocks become increasingly redundant, leading to the observed saturation. Overall, the results indicate that bounded-memory pose stability depends critically on preserving complementary mid-horizon support rather than relying on purely local continuity.

Table 6: Pose estimation results on TUM. Best results are shown in bold.

Method	ATE↓	RPE _t ↓	RPE _r ↓
CUT3R	0.1089	0.0148	0.619
Point3R	0.1387	0.0369	2.347
TTT3R	0.0620	0.0147	0.618
InfiniteVGGT	0.0478	0.0138	0.350
Ours (12)	0.0387	0.0140	0.346
Ours (16)	0.0386	0.0137	0.342
Ours (20)	0.0389	0.0135	0.339
Ours (24)	0.0385	0.0133	0.336

Table 7: Recent ablation on TUM under a fixed total budget ($M_{\text{total}}=16$). Recent-0 corresponds to Ours ($M=16$). Best results are shown in bold.

Sliding Window	ATE↓	RPE _t ↓	RPE _r ↓
Recent-0	0.0386	0.0137	0.342
Recent-2	0.0399	0.0138	0.341
Recent-4	0.0410	0.0140	0.342
Recent-6	0.0432	0.0140	0.341

Recent vs. mid-term evidence. Tab. 7 shows that forcing a Recent- K buffer is insufficient for long-horizon pose stability. Although recency helps short-range continuity, adjacent frames often provide highly overlapping constraints. A larger recent buffer therefore over-allocates memory to near-duplicate local evidence while reducing capacity for more complementary mid-term support. This weakens effective viewpoint and baseline diversity, making it harder to correct drift once local ambiguity accumulates. The resulting increase in ATE and RPE is again consistent with our central claim: long-horizon geometric reasoning depends less on recency alone than on retaining complementary support structure under a fixed memory budget.

4.5 Discussion and Limitations

Across all three tasks, FrameVGGT achieves a consistently better accuracy–memory trade-off under substantially tighter budgets, often matching or exceeding InfiniteVGGT while using only one-quarter to one-half of its memory. These gains are not only about storing less history. Rather, they suggest that under bounded streaming, preserving frame-level support structure is more effective than retaining a larger but more fragmented token set. At the same time, this improvement is achieved without a prohibitive increase in inference cost relative to InfiniteVGGT, while substantially reducing the effective KV-cache footprint.

The results are also consistent with the support-centric view in our analysis. Recent- K ablations show that temporal proximity alone is a poor proxy for geometric utility: recency-biased buffering tends to over-allocate memory to redundant adjacent evidence while reducing complementary mid-term support. Likewise, the observed saturation with increasing memory suggests a finite useful memory scale: once the retained cache already provides sufficiently rich support, additional history contributes diminishing returns and may introduce less useful or weakly aligned evidence.

The anchor study further clarifies the role of the two-tier design. Anchors improve robustness in rare but difficult intervals, but they are not the main source of gains under standard settings. The dominant benefit comes from support-aligned mid-term retention, while anchors act as a lightweight fallback for hard cases.

Limitations and future work. A current limitation is that the memory policy remains fixed during inference: capacity partitioning and update rules are hand-specified rather than adapted to the scene or motion regime. An important next step is therefore to develop adaptive memory control, e.g., reallocating capacity based on scene complexity, motion, or uncertainty. Such policies could make bounded streaming memory more flexible and robust in increasingly diverse environments.

References

- [1] Xingdong Sheng, Shijie Mao, Yichao Yan, and Xiaokang Yang. Review on slam algorithms for augmented reality. *Displays*, 84:102806, 2024.
- [2] Ioan Andrei Bârsan, Peidong Liu, Marc Pollefeys, and Andreas Geiger. Robust dense mapping for large-scale dynamic environments. In *2018 IEEE International Conference on Robotics and Automation (ICRA)*, pages 7510–7517. IEEE, 2018.
- [3] Mehmet Turan, Yusuf Yigit Pilavci, Ipek Ganiyusufoglu, Helder Araujo, Ender Konukoglu, and Metin Sitti. Sparse-then-dense alignment-based 3d map reconstruction method for endoscopic capsule robots. *Machine Vision and Applications*, 29(2):345–359, 2018.

- [4] Ruben Mascaro and Margarita Chli. Scene representations for robotic spatial perception. *Annual Review of Control, Robotics, and Autonomous Systems*, 8(1):351–377, 2025.
- [5] Sonia Raychaudhuri and Angel X Chang. Semantic mapping in indoor embodied ai—a comprehensive survey and future directions. *arXiv preprint arXiv:2501.05750*, 3, 2025.
- [6] Richard A Andersen and David C Bradley. Perception of three-dimensional structure from motion. *Trends in cognitive sciences*, 2(6):222–228, 1998.
- [7] Muhamad Risqi U Saputra, Andrew Markham, and Niki Trigoni. Visual slam and structure from motion in dynamic environments: A survey. *ACM Computing Surveys (CSUR)*, 51(2):1–36, 2018.
- [8] Tanveer Hussain, Khan Muhammad, Weiping Ding, Jaime Lloret, Sung Wook Baik, and Victor Hugo C De Albuquerque. A comprehensive survey of multi-view video summarization. *Pattern Recognition*, 109:107567, 2021.
- [9] Shuzhe Wang, Vincent Leroy, Yohann Cabon, Boris Chidlovskii, and Jerome Revaud. Dust3r: Geometric 3d vision made easy. In *Proceedings of the IEEE/CVF Conference on Computer Vision and Pattern Recognition (CVPR)*, pages 20697–20709, June 2024.
- [10] Bardienus Pieter Duisterhof, Lojze Zust, Philippe Weinzaepfel, Vincent Leroy, Yohann Cabon, and Jerome Revaud. Mast3r-sfm: a fully-integrated solution for unconstrained structure-from-motion. In *2025 International Conference on 3D Vision (3DV)*, pages 1–10. IEEE, 2025.
- [11] Jianyuan Wang, Minghao Chen, Nikita Karaev, Andrea Vedaldi, Christian Rupprecht, and David Novotny. Vggt: Visual geometry grounded transformer. In *Proceedings of the Computer Vision and Pattern Recognition Conference*, pages 5294–5306, 2025.
- [12] Qianqian Wang, Yifei Zhang, Aleksander Holynski, Alexei A Efros, and Angjoo Kanazawa. Continuous 3d perception model with persistent state. In *Proceedings of the Computer Vision and Pattern Recognition Conference*, pages 10510–10522, 2025.
- [13] Xingyu Chen, Yue Chen, Yuliang Xiu, Andreas Geiger, and Anpei Chen. Ttt3r: 3d reconstruction as test-time training. *arXiv preprint arXiv:2509.26645*, 2025.
- [14] Dong Zhuo, Wenzhao Zheng, Jiahe Guo, Yuqi Wu, Jie Zhou, and Jiwen Lu. Streaming 4d visual geometry transformer. *arXiv preprint arXiv:2507.11539*, 2025.
- [15] Shuai Yuan, Yantai Yang, Xiaotian Yang, Xupeng Zhang, Zhonghao Zhao, Lingming Zhang, and Zhipeng Zhang. Infinitveggt: Visual geometry grounded transformer for endless streams. *arXiv preprint arXiv:2601.02281*, 2026.
- [16] Sameer Agarwal, Yasutaka Furukawa, Noah Snavely, Ian Simon, Brian Curless, Steven M Seitz, and Richard Szeliski. Building rome in a day. *Communications of the ACM*, 54(10):105–112, 2011.
- [17] Johannes L Schonberger and Jan-Michael Frahm. Structure-from-motion revisited. In *Proceedings of the IEEE conference on computer vision and pattern recognition*, pages 4104–4113, 2016.
- [18] Yasutaka Furukawa and Carlos Hernández. Multi-view stereo: A tutorial. *Foundations and Trends in Computer Graphics and Vision*, 9(1-2):1–148, 2015.
- [19] Fan Zhu, Ziyu Chen, Chunmao Jiang, Liwei Xu, Shijin Zhang, Biao Yu, and Hui Zhu. Slm-slam: a visual slam system based on segmented large-scale model in dynamic scenes and zero-shot conditions. *Measurement Science and Technology*, 35(8):086315, 2024.
- [20] Raul Mur-Artal, Jose Maria Martinez Montiel, and Juan D Tardos. Orb-slam: A versatile and accurate monocular slam system. *IEEE transactions on robotics*, 31(5):1147–1163, 2015.
- [21] Takafumi Taketomi, Hideaki Uchiyama, and Sei Ikeda. Visual slam algorithms: A survey from 2010 to 2016. *IPSN transactions on computer vision and applications*, 9(1):16, 2017.
- [22] Kai Deng, Zexin Ti, Jiawei Xu, Jian Yang, and Jin Xie. Vggt-long: Chunk it, loop it, align it—pushing vggt’s limits on kilometer-scale long rgb sequences. *arXiv preprint arXiv:2507.16443*, 2025.
- [23] Junyuan Deng, Heng Li, Tao Xie, Weiqiang Ren, Qian Zhang, Ping Tan, and Xiaoyang Guo. Sail-recon: Large sfm by augmenting scene regression with localization. *arXiv preprint arXiv:2508.17972*, 2025.
- [24] Hengyi Wang and Lourdes Agapito. 3d reconstruction with spatial memory. In *2025 International Conference on 3D Vision (3DV)*, pages 78–89. IEEE, 2025.

- [25] Yuqi Wu, Wenzhao Zheng, Jie Zhou, and Jiwen Lu. Point3r: Streaming 3d reconstruction with explicit spatial pointer memory. *arXiv preprint arXiv:2507.02863*, 2025.
- [26] Zhuoguang Chen, Minghui Qin, Tianyuan Yuan, Zhe Liu, and Hang Zhao. Long3r: Long sequence streaming 3d reconstruction. In *Proceedings of the IEEE/CVF International Conference on Computer Vision*, pages 5273–5284, 2025.
- [27] Zizun Li, Jianjun Zhou, Yifan Wang, Haoyu Guo, Wenzheng Chang, Yang Zhou, Haoyi Zhu, Junyi Chen, Chunhua Shen, and Tong He. Wint3r: Window-based streaming reconstruction with camera token pool. *arXiv preprint arXiv:2509.05296*, 2025.
- [28] Hunter Blanton, Connor Greenwell, Scott Workman, and Nathan Jacobs. Extending absolute pose regression to multiple scenes. In *Proceedings of the IEEE/CVF Conference on Computer Vision and Pattern Recognition Workshops*, pages 38–39, 2020.
- [29] Dejan Azinović, Ricardo Martin-Brualla, Dan B Goldman, Matthias Nießner, and Justus Thies. Neural rgb-d surface reconstruction. In *Proceedings of the IEEE/CVF conference on computer vision and pattern recognition*, pages 6290–6301, 2022.
- [30] Emanuele Palazzolo, Jens Behley, Philipp Lottes, Philippe Giguere, and Cyrill Stachniss. Refusion: 3d reconstruction in dynamic environments for rgb-d cameras exploiting residuals. In *2019 IEEE/RSJ International Conference on Intelligent Robots and Systems (IROS)*, pages 7855–7862. IEEE, 2019.
- [31] Jürgen Sturm, Nikolas Engelhard, Felix Endres, Wolfram Burgard, and Daniel Cremers. A benchmark for the evaluation of rgb-d slam systems. In *2012 IEEE/RSJ International Conference on Intelligent Robots and Systems*, pages 573–580, 2012.

A Why Token-Level Compression is Less Suitable for Geometric Streaming

This appendix provides a proxy-based analytical perspective on why *token-level retention* can become less suitable for long-horizon geometric streaming under bounded memory. Our goal is not to establish an impossibility theorem for token pruning, but to clarify a structural mismatch between fine-grained token selection and the multi-view support structure required by geometric inference.

Unlike language modeling, where semantic content can often be preserved by a small set of salient tokens, geometric estimation is fundamentally relational: stable depth and pose inference rely on repeated and spatially distributed observations across views. Under bounded memory, aggressive token-level pruning may preserve the nominal token count while progressively weakening the non-degenerate support required for reliable geometric reasoning.

We analyze this mismatch through three coupled mechanisms: (1) *support thinning*, where bounded budgets reduce the usable evidence retained per frame, (2) *spatio-temporal decoupling*, where multi-view support relationships become fragmented across time, and (3) *bias amplification*, where sparse memory increases the sensitivity of attention-based fusion to a small subset of retained tokens.

A.1 Problem Setup

Consider a video stream of length T . Frame t produces N_t tokens

$$X_t = \{x_{t,1}, \dots, x_{t,N_t}\}, \quad x_{t,i} \in \mathbb{R}^d. \quad (12)$$

A bounded-memory policy retains tokens using indicators $m_{t,i} \in \{0, 1\}$. The retained set is

$$\tilde{X}_t = \{x_{t,i} : m_{t,i} = 1\}, \quad b_t = \sum_{i=1}^{N_t} m_{t,i}, \quad (13)$$

where b_t denotes the retained token count of frame t . The global KV cache is constrained by

$$\sum_{t=1}^T \sum_{i=1}^{N_t} m_{t,i} \leq M. \quad (14)$$

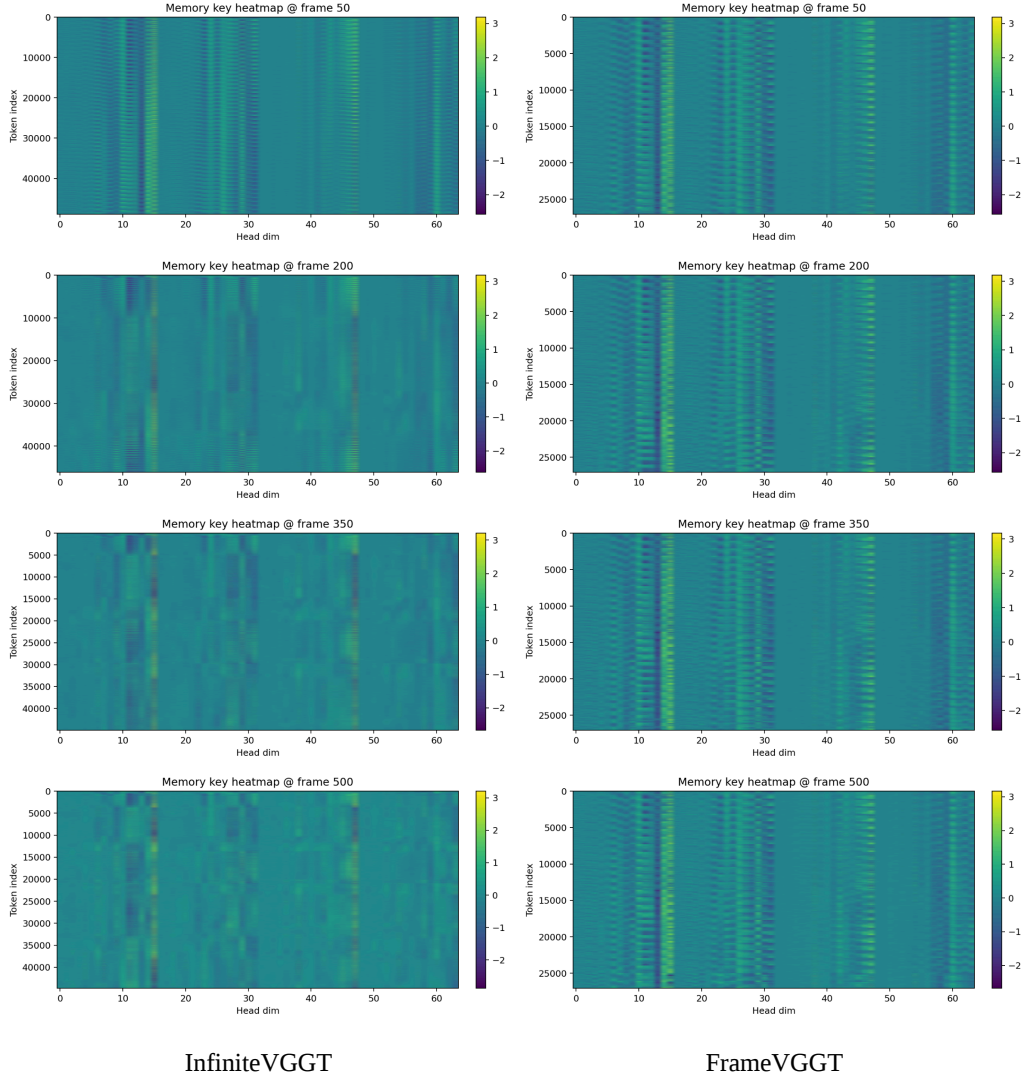


Figure 5: Visualization of memory-key heatmaps at different timesteps. Left: InfiniteVGGT. Right: FrameVGGT. Heatmaps visualize saved memory key snapshots at different checkpoints. Rows are retained memory tokens (internal memory order) and columns are key dimensions (one layer/head slice; batch=0 and head=0 when applicable). Color encodes the key value; the colorbar is auto-scaled per snapshot (ticks chosen automatically), so absolute intensities are not directly comparable across checkpoints. Banded patterns indicate groups of tokens with similar key profiles (higher row-wise correlation), while diffuse patterns indicate more heterogeneous keys.

The key issue is not merely how many tokens are retained globally, but whether the retained memory still preserves the *geometrically usable support* required for inference.

Support proxy. Let

$$S_t^* = S(X_t), \quad S_t = S(\tilde{X}_t) \quad (15)$$

denote the usable geometric support before and after compression, respectively. The function $S(\cdot)$ is a task-level proxy capturing whether retained observations provide sufficient non-degenerate geometric constraints. Possible instantiations include spatial coverage, epipolar inlier support, reprojection consistency, or covariance-rank surrogates.

We define the *support damage*

$$D_t = S_t^* - S_t \geq 0. \quad (16)$$

Thus the retained token count measures *compression*, while D_t measures the degradation of usable geometric evidence.

For convenience we also define the effective support ratio

$$\rho_t = \frac{S_t}{S_t^*} \in [0, 1]. \quad (17)$$

Importantly, compression ratio and support preservation need not be proportional.

A.2 Compression Ratio and Support Thinning

Define the per-frame compression ratio

$$c_t = 1 - \frac{b_t}{N_t}. \quad (18)$$

The global budget immediately implies the following property.

Proposition A.1 (Average retained tokens under bounded memory). *Under the global constraint (14),*

$$\frac{1}{T} \sum_{t=1}^T b_t \leq \frac{M}{T}. \quad (19)$$

In particular, for fixed M , the average retained tokens per frame vanish as $T \rightarrow \infty$.

Proof. Summing $b_t = \sum_i m_{t,i}$ over t gives

$$\sum_{t=1}^T b_t = \sum_{t=1}^T \sum_{i=1}^{N_t} m_{t,i} \leq M.$$

Dividing by T yields the claim. □

This result makes explicit that bounded streaming inevitably induces *support thinning*: as the horizon grows, the retained evidence must be spread over more and more source frames, so the average amount of memory available to each frame shrinks.

A concrete way to interpret Proposition A.1 is through the effective per-frame retention rate. Suppose a token-level policy distributes its bounded memory roughly across all previously seen frames. Then as the sequence length increases, each frame can only keep a progressively smaller fraction of its original evidence. In our experiments, this effect is already severe at moderate horizons: by around 200 frames, the retained memory corresponds to roughly only 25% of the original tokens per frame on average, i.e., about 75% are compressed away; by 500 frames, only about 10% remain on average, meaning roughly 90% of the per-frame evidence has been discarded. This is not a mild compression regime. For geometric streaming, such a level of thinning is close to destructive, because it removes most of the repeated observations that normally provide stable multi-view support.

Importantly, geometric degradation is governed not only by the compression ratio itself, but by the induced support damage D_t . Two policies may retain a similar number of tokens while producing very different usable support densities ρ_t . In particular, token-level pruning can remove observations that appear redundant at the token level but are in fact jointly important for geometric stabilization, leading to disproportionately large support damage relative to the nominal compression rate.

A.3 Spatio-Temporal Decoupling of Multi-View Support

Geometric inference depends not only on how many tokens survive, but on whether the surviving observations still form coherent cross-view support. Depth and pose estimation rely on correlated evidence across nearby frames, such as repeated observations of the same surface patch, consistent parallax, and jointly usable correspondences for triangulation or reprojection alignment.

Token-level pruning operates independently at fine granularity and is not explicitly constrained to preserve such structures. As a result, even when some salient tokens remain in each frame, they may no longer overlap in a way that supports stable multi-view reasoning. For example, after aggressive compression, frame t may retain a few tokens on one object boundary, while frame $t + 1$ retains tokens from a different region, and frame $t + 2$ keeps only sparse texture fragments. Although each frame is still represented by some surviving tokens, the sequence of retained evidence no longer forms a coherent observation chain of the same 3D structure. The memory is therefore present in quantity, but broken in geometry.

This is the sense in which bounded token-level retention causes *spatio-temporal decoupling*: the budget is globally respected, yet the support required for joint geometric estimation becomes fragmented across both space and time. Under moderate horizons this already becomes problematic, and under long horizons it can be catastrophic. In the regime observed in our experiments, where the average per-frame compression reaches roughly 75% at 200 frames and 90% at 500 frames, the retained token set becomes too thin to reliably preserve dense local overlap across views. What remains is often a scattered collection of isolated fragments rather than a structurally usable support set.

Qualitatively, this interpretation is consistent with the memory-key heatmaps in Fig. 5. FrameVGGT preserves clearer banded structures over time, suggesting that memory remains organized as coherent frame-level evidence blocks. In contrast, token-level retention produces increasingly diffuse patterns, consistent with a memory state that is spread thinly over many frames while losing within-frame and cross-frame structural coherence. From a geometric perspective, this is highly destructive: once support is both thinned and decoupled, downstream retrieval may still access memory, but the retrieved evidence is no longer sufficient to stably constrain the underlying 3D scene.

A.4 Bias Amplification Under Weak Redundancy

Support thinning alone does not fully explain degradation, since retained memory is later consumed through key-query attention. When redundancy decreases, inference becomes more sensitive to a small subset of surviving tokens.

Let $\hat{k}_{t,i} = k_{t,i}/\|k_{t,i}\|$ denote normalized keys. For time k , let R_k denote a subset of keys associated with the dominant local support regime, and N_k the remaining keys. Define

$$\mu_R = \frac{\frac{1}{|R_k|} \sum_{i \in R_k} \hat{k}_i}{\left\| \frac{1}{|R_k|} \sum_{i \in R_k} \hat{k}_i \right\|}. \quad (20)$$

We introduce the contrast statistic

$$\Delta_k = \frac{1}{|R_k|} \sum_{i \in R_k} \cos(\hat{k}_i, \mu_R) - \frac{1}{|N_k|} \sum_{j \in N_k} \cos(\hat{k}_j, \mu_R). \quad (21)$$

This quantity summarizes how strongly retained keys concentrate around a narrow dominant direction relative to the rest of memory. Larger and increasing Δ_k indicates that fusion relies increasingly on a small subset of tokens.

The effect can be understood through the attention weights

$$z_i = \langle q_k, \hat{k}_i \rangle / \sqrt{d}, \quad a_i = \frac{e^{z_i}}{\sum_j e^{z_j}}. \quad (22)$$

When redundant observations are present, multiple compatible tokens jointly stabilize the attention output. When redundancy is reduced, small perturbations in a few tokens can dominate the softmax, amplifying noise or mismatch.

We therefore interpret increasing Δ_k as an empirical indicator of growing fusion brittleness. Figure 6 illustrates its temporal evolution.

A.5 Frame-Level Retention as Structural Preservation

The preceding analysis suggests that the key issue is not simply how many tokens are retained, but whether retained memory preserves coherent geometric support units.

Frame-level retention addresses this by preserving each frame’s KV contribution as a coherent evidence block. This encourages the retained memory to maintain spatial coverage, viewpoint diversity, and local parallax structure.

From this perspective,

token-level retention \approx unstructured pruning,

while

frame-level retention \approx structural preservation.

For comparable compression ratios, block-level policies tend to maintain higher support ratios ρ_t and smaller support damage D_t , making the resulting memory more suitable for stable geometric reasoning.

A.6 Finite Useful Memory Scale

Finally, the analysis also explains why increasing memory may exhibit diminishing returns.

When memory is extremely small, performance is limited by support availability: increasing M reduces support thinning and improves ρ_t . Beyond a task-dependent scale, however, additional memory primarily introduces stale or weakly aligned observations that contribute little to conditioning the geometric problem.

This saturation effect is typically more pronounced for token-level policies, which allow memory to spread over many partially informative fragments. Frame-level policies, by contrast, constrain retention to support-aligned units and therefore exhibit smoother scaling behavior under bounded streaming.

B Design Principles: Retrieval-Centric Memory Selection

We formulate mid-term memory selection as a bounded coverage problem in transformer retrieval space. Given a candidate set of frame-wise KV blocks M_t , the goal is to retain a subset that preserves broad coverage of *retrievable* geometric evidence under a fixed budget.

Why key space? In attention-based memory, Keys and Values play asymmetric roles: Keys determine how memory is addressed by future queries, while Values provide the retrieved content. Accordingly, redundancy for memory selection is most naturally measured in key space. By summarizing each frame’s incremental KV contribution into a prototype $v_t^{(l)}$, we obtain a compact descriptor of its retrieval direction while preserving block-level coherence.

Why cosine dissimilarity? We compare normalized block prototypes by

$$d(B_i^{(l)}, B_j^{(l)}) = 1 - \langle \bar{v}_i^{(l)}, \bar{v}_j^{(l)} \rangle, \quad (23)$$

where $\bar{v}_i^{(l)} = v_i^{(l)} / \|v_i^{(l)}\|_2$. Cosine dissimilarity is appropriate because it is scale-invariant and directly measures directional similarity in retrieval space. Thus, blocks that are close under $d(\cdot, \cdot)$ are expected to induce similar retrieval behavior and can be treated as redundant under a bounded budget.

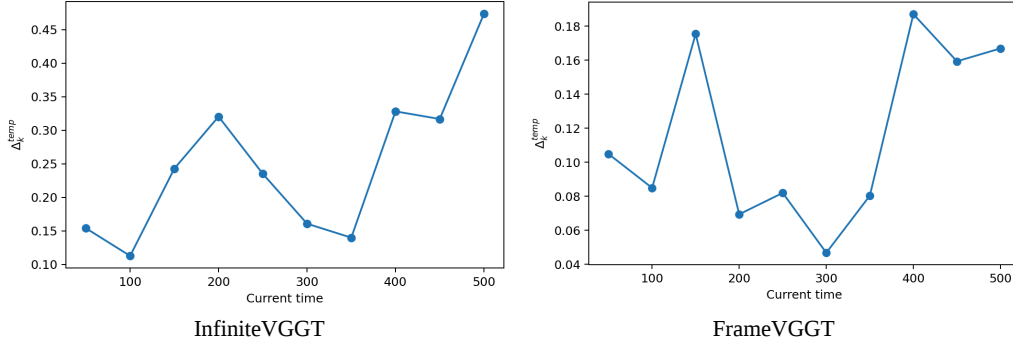


Figure 6: Temporal evolution of the contrast statistic Δ_k under bounded streaming memory. Larger and progressively increasing Δ_k indicates stronger concentration around a narrow dominant key direction and a potentially more brittle fusion regime. Token-level retention exhibits both higher Δ_k and stronger temporal growth, suggesting increasing sensitivity to a small subset of retained keys over long streams. By contrast, FrameVGGT maintains a flatter and more stable trajectory, consistent with better-balanced fusion under the same bounded-memory regime.

Table 8: Reconstruction results on 7-Scenes and NRGBD. Best results are shown in bold.

Method	7-Scenes						NRGBD					
	Acc↓	Acc _{med} ↓	Comp↓	Comp _{med} ↓	NC↑	NC _{med} ↑	Acc↓	Acc _{med} ↓	Comp↓	Comp _{med} ↓	NC↑	NC _{med} ↑
Ours (Without Anchor)	0.028	0.009	0.019	0.0040	0.564	0.598	0.054	0.035	0.030	0.0060	0.670	0.782
Ours (With Anchor)	0.026	0.009	0.018	0.0040	0.571	0.607	0.053	0.034	0.031	0.0057	0.682	0.793

Why metric k -center? To enforce a bounded mid-term bank of capacity B_M , we select

$$S^* = \arg \min_{S \subseteq M_t, |S| \leq B_M} \max_{B \in M_t} \min_{B' \in S} d(B, B'). \quad (24)$$

This metric k -center objective minimizes the worst-case coverage gap from any candidate block to the retained subset, favoring complementary representatives over near-duplicate observations. In streaming geometry, where adjacent frames are often highly redundant, such coverage control is better aligned with long-horizon support preservation than recency-only retention.

Greedy approximation and complexity. We approximate this objective by greedy farthest-first traversal, initialized from the most recent block to preserve immediate relevance. For efficiency, we maintain

$$m(B) = \min_{B' \in S} d(B, B'), \quad (25)$$

and update it after selecting a new center B_{new} :

$$m(B) \leftarrow \min(m(B), d(B, B_{\text{new}})). \quad (26)$$

This preserves the same selection rule while avoiding repeated recomputation.

Let $n = |M_t|$ and $k = B_M$. Prototype construction costs $O(H|T_t|D)$ per new block, and greedy selection costs $O(knD)$ with $O(n)$ auxiliary memory. Because selection is performed on frame/block prototypes rather than individual tokens, the added overhead remains modest relative to backbone inference.

C Additional Reconstruction Visualization

Before turning to pose trajectories, we further examine the long-horizon behavior of reconstructed geometry. Compared with per-frame depth maps, reconstruction renderings provide a more direct view of whether the retained memory preserves *global structural consistency* as evidence accumulates over time.

Fig. 7 presents additional qualitative reconstruction results on 7-Scenes and NRGBD. Across extended streaming horizons, the reconstructed geometry remains visually coherent: dominant planes, major

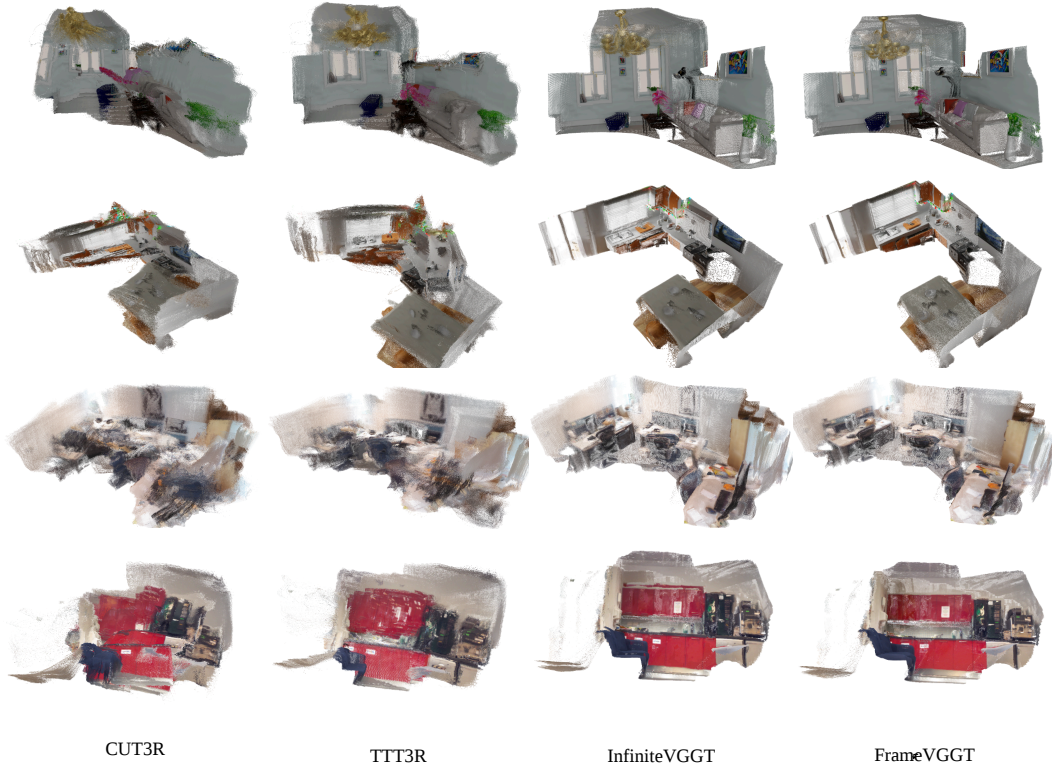


Figure 7: Additional reconstruction visualizations on 7-Scenes and NRGBD. We show representative renderings from FrameVGGT over extended streaming sequences. These examples complement the quantitative reconstruction results in the main paper by illustrating long-horizon structural consistency under bounded memory.

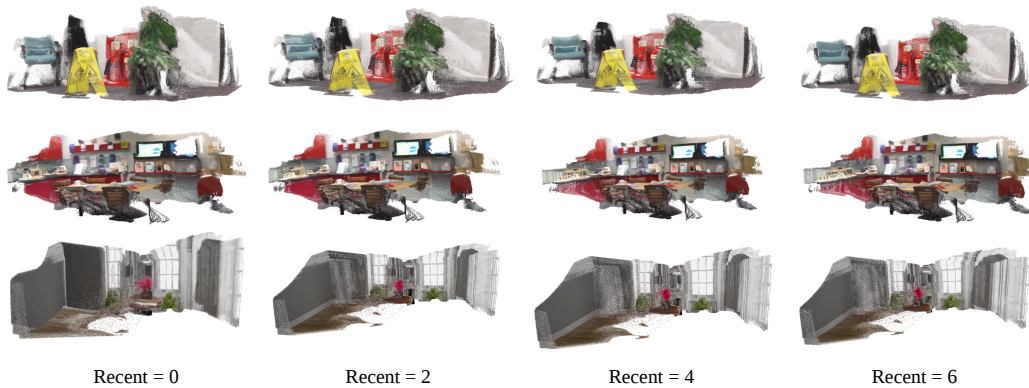


Figure 8: Additional reconstruction visualizations with **recent-only** memory on 7-Scenes and NRGBD.

scene boundaries, and overall layout structure are stably preserved. Although regions with weaker multi-view support may exhibit mild local uncertainty as the sequence grows, we do not observe large-scale structural collapse or severe global distortion. This suggests that the retained memory continues to preserve sufficiently coherent geometric support even in prolonged streaming regimes.

To further isolate the role of memory structure, Figs. 8–10 compare three retention regimes: **recent-only**, **mid-term**, and the **global anchor tier**.

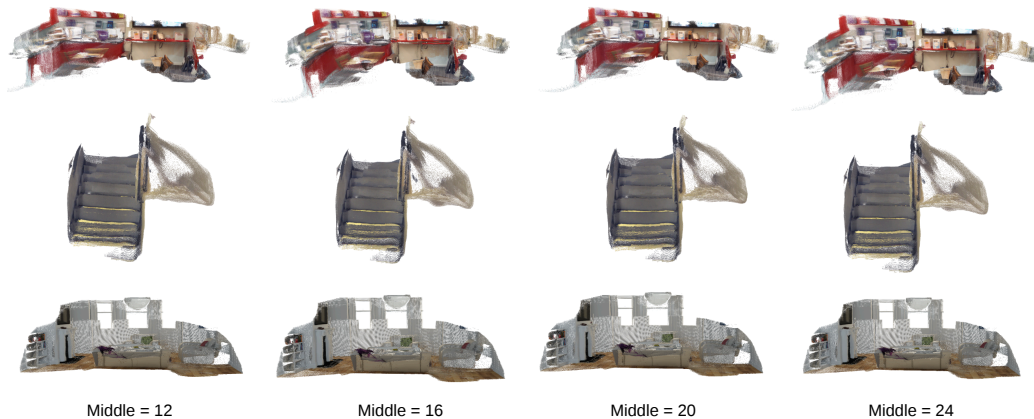


Figure 9: Additional reconstruction visualizations with **mid-term** memory on 7-Scenes and NRGBD.

Recent-only memory (Fig. 8). When memory is concentrated on only the most recent observations, reconstruction is driven primarily by short-range temporal continuity. This often suffices in early segments, where adjacent views still provide dense local support. However, as the horizon extends, the lack of longer-range geometric witnesses makes the reconstruction increasingly vulnerable to accumulated drift, duplication artifacts, and weakened global consistency. In our framework, this corresponds to a regime where local support remains available but the broader geometric skeleton of the scene is no longer sufficiently preserved.

Mid-term memory (Fig. 9). Retaining mid-horizon context substantially improves long-range stability by preserving additional support from intermediate temporal neighborhoods. Compared with the recent-only regime, dominant structures are more consistently maintained and drift accumulation is visibly reduced. This indicates that memory aligned with intermediate-range support is more effective at sustaining global reconstruction coherence. Nevertheless, when the sequence extends well beyond the effective temporal span of the mid-term bank, residual artifacts can still emerge, reflecting the finite coverage of a bounded but non-global memory tier.

Global anchor tier (Fig. 10). Introducing the global anchor tier further strengthens reconstruction stability by preserving sparse but persistent long-horizon reference frames. Qualitatively, anchors help suppress duplication artifacts, stabilize scene layout, and better maintain a consistent global structure over extended horizons. In effect, the anchor tier acts as a sparse geometric skeleton that complements the online mid-term pathway with globally distributed reference points. This qualitative trend is also reflected quantitatively in Tab. 8: introducing anchors preserves comparable performance on clean or easier sequences while improving robustness on more challenging cases, where long-horizon drift and structural duplication are more likely to accumulate. Thus, the anchor tier improves hard-case stability without sacrificing performance in well-conditioned streams.

Overall, these additional visualizations suggest that long-horizon reconstruction quality depends not only on the amount of retained evidence, but more fundamentally on the *temporal structure* of that evidence. Structured retention better preserves the support organization required for stable geometry, which in turn yields stronger long-range reconstruction consistency. These observations are consistent with the trajectory behavior analyzed next.

D Additional Depth Visualization

Before analyzing pose trajectories, we first examine the long-horizon behavior of predicted depth. Depth stability provides a direct proxy for whether the retained memory continues to preserve sufficiently coherent local geometric support over time.

Unlike pose trajectories, depth visualizations across different methods are not strictly comparable in a fully fair manner because of scale-shift ambiguity, normalization differences, and colormap choices.

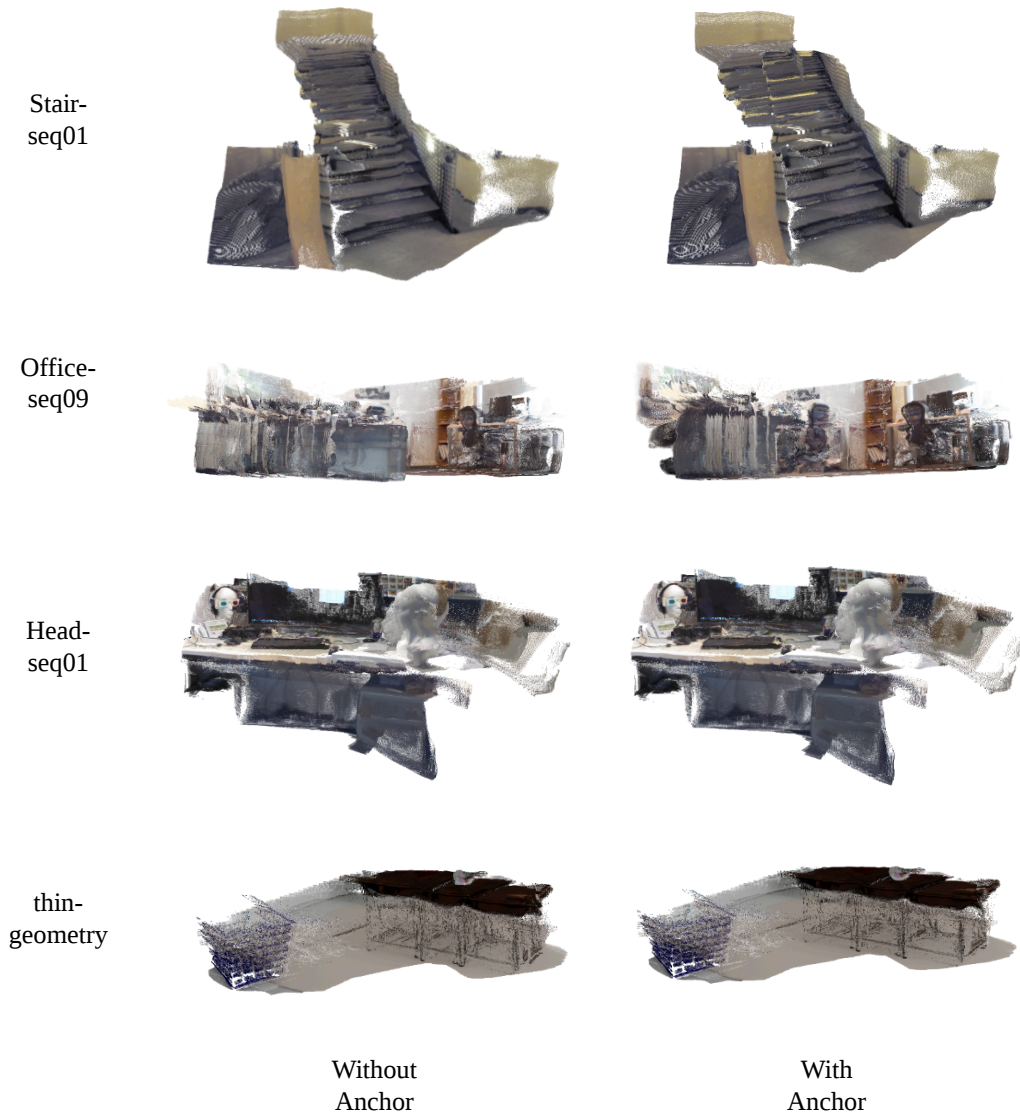


Figure 10: Additional reconstruction visualizations with the **global anchor tier** on 7-Scenes and NRGBD.

We therefore focus on the temporal behavior of FrameVGGT itself rather than presenting side-by-side method comparisons.

Fig. 11 shows representative depth maps across extended streaming sequences on BONN. In early segments, the predicted geometry is sharp and spatially coherent. As time progresses, regions with weaker multi-view support may exhibit mild local uncertainty; however, large-scale structural collapse, catastrophic distortion, or obvious degeneration of dominant layouts is not observed. Major planes and scene boundaries remain temporally stable over long horizons, indicating that the retained memory continues to provide sufficiently concentrated support for depth inference.

These qualitative observations are consistent with the intended role of structured memory retention: preserving informative mid-horizon context helps maintain local geometric coherence even as the stream becomes progressively longer. This depth-level stability forms the geometric basis for the trajectory behavior analyzed next.

E Additional Pose Visualization

To further characterize long-horizon pose behavior beyond aggregate metrics, we provide additional qualitative trajectory visualizations on TUM in Fig. 12, together with focused comparisons of different retention regimes in Figs. 13a and 13b. These figures serve as qualitative evidence of how bounded-memory structure affects long-range trajectory stability.

Fig. 12 compares representative long-sequence trajectories across methods. A consistent pattern is that deviations from the global trajectory shape accumulate over time: many baselines remain reasonably stable in earlier segments but exhibit increasingly visible drift in later portions of the sequence. Although the precise failure signatures vary—for example, gradual drift versus abrupt deviation—the common trend is the progressive erosion of global consistency under long-horizon bounded streaming.

Figs. 13a and 13b isolate the role of temporal retention structure. The *mid-term* regime preserves intermediate-range history, which provides complementary constraints once motion extends beyond immediate neighbors. This additional support helps stabilize the trajectory against drift that cannot be corrected using only near-adjacent evidence. In contrast, the *recent-only* regime concentrates capacity on short-range observations. While this often preserves local continuity, it provides weaker constraints on long-horizon global consistency, especially when viewpoint diversity or baseline growth requires support from a broader temporal neighborhood.

Overall, these qualitative examples align with the quantitative results in the main paper: preserving informative mid-horizon context improves long-range trajectory stability by better maintaining the geometric support structure needed for consistent pose estimation over extended streams.

F KV-Cache Budget and Memory Accounting

To ensure fair comparison across different memory policies, all methods in our experiments operate under comparable KV-cache budget settings. In particular, memory usage is measured by the effective footprint of the retained Transformer KV cache during streaming inference.

For a Transformer layer l , the KV cache size is proportional to

$$\text{Mem}_{KV}^{(l)} \propto H_l T_l D_l \times 2, \tag{27}$$

where H_l is the number of attention heads, T_l the number of retained tokens, and D_l the feature dimension per head; the factor of 2 accounts for keys and values. Total KV-cache memory is obtained by summing this quantity across all layers.

Although different methods organize memory differently (e.g., token-level vs. frame/block-level retention), the reported memory footprint always reflects the actual retained KV tensors used during inference. Thus, comparisons across methods correspond to comparable KV-cache budgets rather than unequal GPU allocations.

Unless otherwise stated, the reported memory usage excludes unrelated overheads such as dataset loading, visualization buffers, or evaluation pipelines, and reflects only the effective KV-cache footprint of the streaming model.

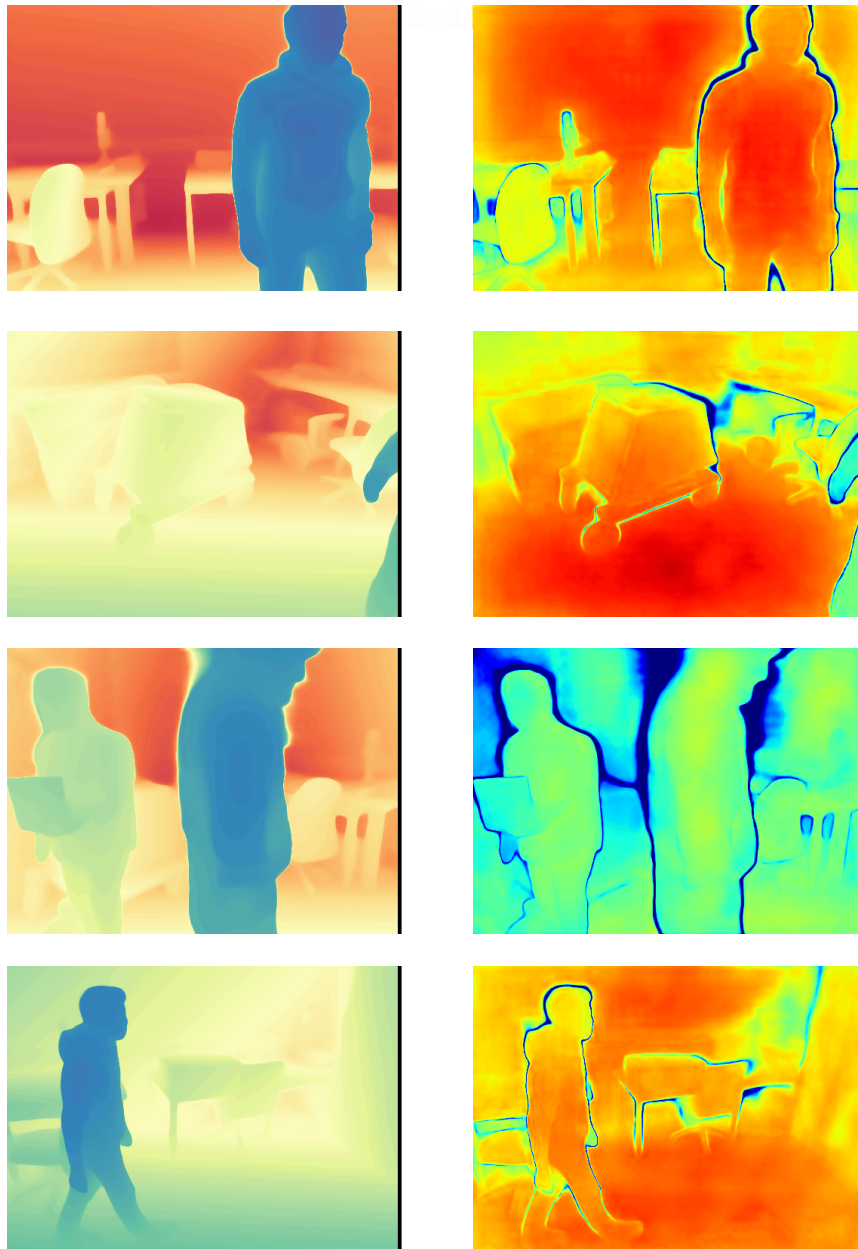


Figure 11: Additional depth visualization results on BONN. We visualize predicted depth maps from FrameVGGT over extended streaming sequences.

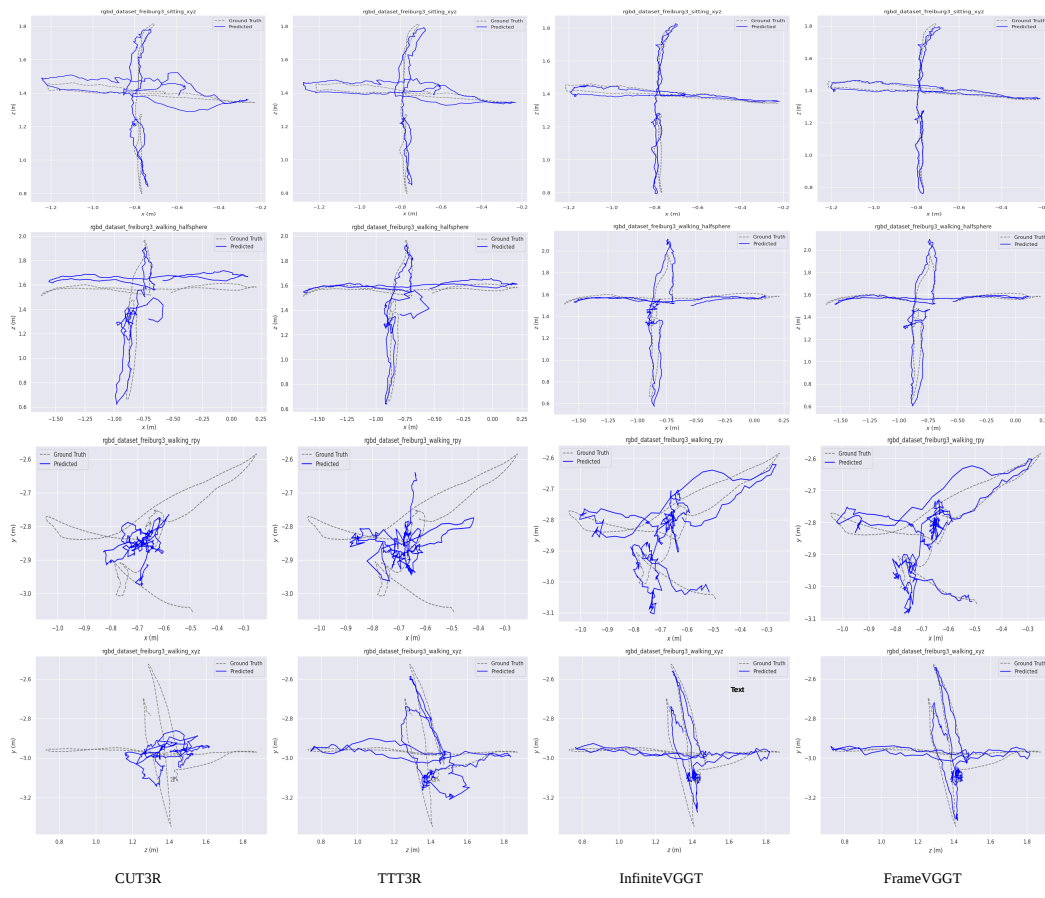
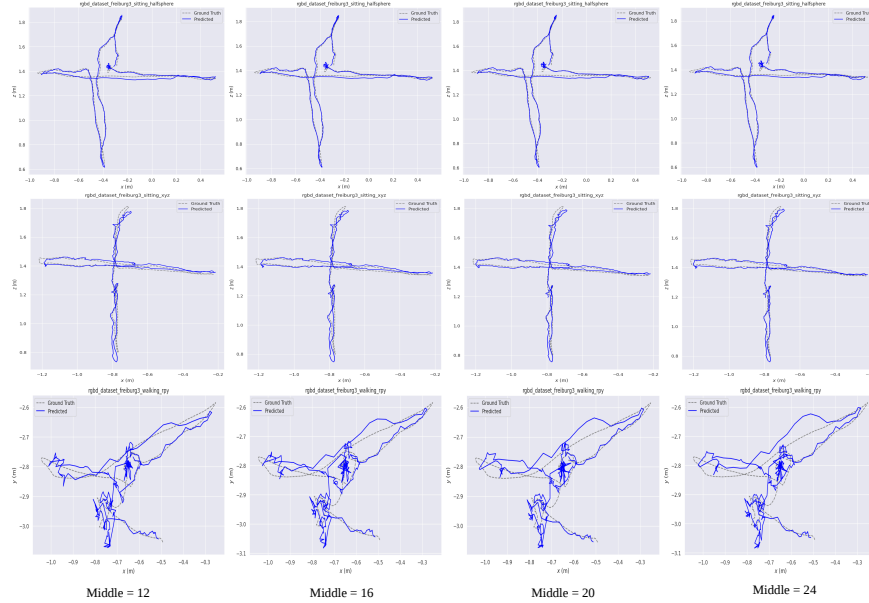
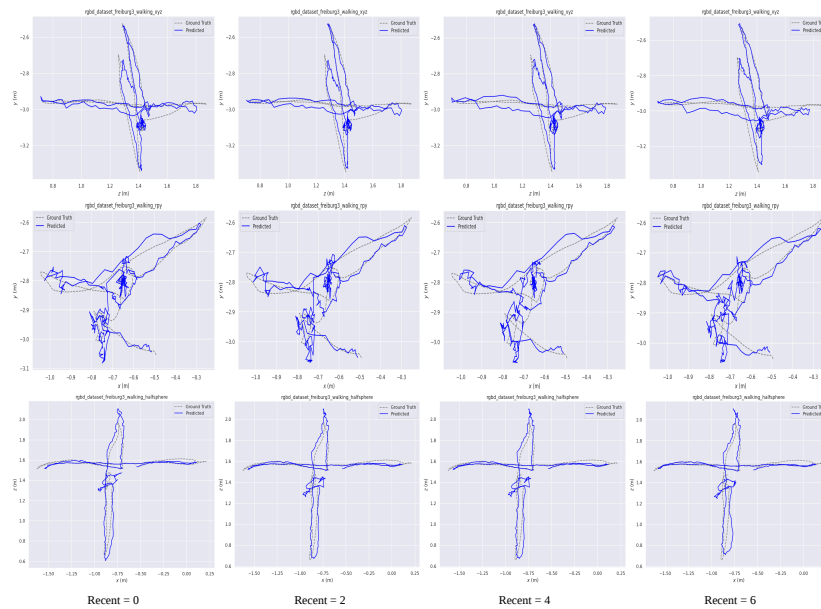


Figure 12: Additional pose visualization results on the TUM dataset. The figure shows representative trajectory comparisons over longer sequences.



(a) Additional visualization focusing on the behavior of the mid-term memory regime. Preserving intermediate-range history provides stronger temporal support beyond the immediate local context.



(b) Additional visualization focusing on the behavior of the recent-memory regime. Retaining only recent observations is effective for short-range continuity but offers limited support over extended horizons.